Journal of Computational Applied Mechanics 2025, 56(2): 380-395

DOI: 10.22059/jcamech.2025.388665.1336

RESEARCH PAPER

MHD nanofluid flow and heat transfer past a horizontal stretching cylinder in Darcy porous medium in presence of slip and uniform/variable wall temperature

Sudip Dey [a], Swati Mukhopadhyay [a,*], Kuppalapalle Vajravelu [b]

[a] *Department of Mathematics, The University of Burdwan, Burdwan-713104, W.B., India*
[b] *Department of Mathematics, Department of Mechanical, Materials& Aerospace Engineering, University of Central Florida, Orlando, FL 32816-1364, USA*

Abstract

The steady magnetohydrodynamics (MHD) axisymmetric flow of nanofluid and heat transfer past a horizontal stretching cylinder embedded in porous medium in presence of velocity slip has been investigated. In this study, aluminum oxide nanoparticles are dropped in base fluid: water to make nanofluid. Applications of similarity transformations convert the partial differential equations corresponding to the momentum and heat equations into highly non-linear ordinary differential equations. Numerical solutions are obtained using the shooting technique with Runge-Kutta method. The influence magnetic field, porous medium, curvature parameter, slip and nanofluid volume fraction on velocity and temperature are analyzed in detail. The results show that an increase in the slip parameter leads to an augmentation in the fluid flow away from the wall and also in heat transfer characteristics. When the volume fraction of nanoparticles increases and the slip increases, the heat transfer rate declines, but the heat transfer is enhanced when the curvature parameter rises. This work brings valuable perceptions on the behavior of nanofluids which have wider engineering applications particularly in heat transfer improvement and flow control around cylindrical surfaces.

Keywords: Nanofluid; MHD; stretching cylinder; Darcy porous medium; velocity slip.

1. Introduction

Heat transfer is a vital area of research which has wider applications in several fields mostly in thermal engineering. Heat transfer also plays a vital role in industrial growth as exchange of effective thermal energy is essential for industrial facility. In recent years, the use of nanofluids is remarkably increased in industrial sectors as it is used now-a-days as an advanced approach of enhancing heat transfer [1-6]. This novel concept of nanofluids was first introduced by Choi [7]. Xuan and Li [8] examined the enhancement of heat transfer efficiency through the use of nanofluids.Convective heat transfer of a Cu-water nanofluid passing through a circular tube was explored by Heris et al. [9]. Mukhopadhyay[10]studied characteristics of heat transfer for unsteady MHD flow over a non-isothermal stretching surface. Study of flow and heat transfer of Williamson nanofluid was inspected by Nadeem

* Corresponding author. *Email address:* swati_bumath@yahoo.co.in

and Hussain[11].

Porous media is a surface containing several voids filled with fluid and has vast applications in several industrial processes like evaporative freezing, reverse osmosis, heterogeneous catalysts, processing of crude oil, casting, etc. [12]. To enhance the heat transport in industrial sectors, recently, the use of porous media has been started [13]. Basically, due to presence of porous media, the contact area of solid-liquid surface increases [13]. Conversely, the effective thermal conductivity of nanofluid is enhanced due to the dispersion of nanoparticles [13]. Thus, it is expected that use of porous media and nanofluid can noticeably enhance the competence of usual thermal systems [13] .

No-slip boundary condition (the supposition that a liquid adheres to a solid boundary) is one of the central tenets. There are certain circumstances where no-slip boundary condition does not hold. A phenomenon known as velocity slip has been detected in certain situations when fluids fail to adhere to the solid borders. Andersson [14] studied the flow over a stretching surface in presence of slip. Abbas et al. [15] reviewed the influences of slip and heat movement in a viscous fluid past an oscillatory stretching surface. Mukhopadhyay [16] inspected heat transfer for unsteady mixed convection flow with slip over a porous stretching surface. Gbadeyan et al. [17] scrutinized the impact of variable thermal conductivity and viscosity on Casson nanofluid flow providing critical perceptions connected to convective heating and velocity slip conditions.

The flow and heat allocation of a viscous fluid in presence of magnetic field have widespread applications in several engineering fields, including MHD power generation, plasma research, petroleum processes and boundary layer management in aerodynamics. To control the boundary layer behaviour, numerous artificial procedures have been invented, among which the application of MHD principles stands out as an important method for operating the flow field and adjusting the boundary layer structure. Sheikholeslami et al. [18] explored the influences of thermal radiation on flow and heat transfer of MHD nanofluids via a two-phase model. Ghosh and Mukhopadhyay [19] reviewed the MHD Casson nanofluid flow past an exponentially stretching permeable sheet in presence of slip. Dey and Mukhopadhyay [20] inspected the flow of MHD nanofluid over a plate with chemical reaction and zero nanoparticle flux. Khan et al. [21] explored the heat and mass transport for MHD flow of Williamson nanofluid past a stretching sheet.

The study of hydrodynamic flow and heat transport due to stretching surfaces, such as cylinders, have drawn interest of the researchers due to their importance in engineering sectors and also for crucial role in developments of several technological items [22-24]. Wang [25] studied fluid flow past a stretching cylinder. Ishak et al. [26] reported the consequences of fluid flow and heat movement over a stretching cylinder considering the impacts of uniform suction or blowing. Mukhopadhyay [27] carefully examined magnetohydrodynamics (MHD) boundary layer slip flow past a stretching cylinder. Ashorynejad et al. [28] inspected the flow of MHD nanofluid and heat transfer owing to a stretching cylinder. Flow of Casson fluid past a stretching cylinder in presence of magnetic field was examined by Tamoor et al. [29]. Mishra and Kumar [30] studied the impacts of velocity and thermal slips on MHD nanofluid flow due to a stretching cylinder. They also reported the influences of Joule heating and viscous dissipation. Sowmiya and Kumar [31] explored the behaviour of MHD flow of Maxwell nanofluid due to a stretching cylinder within a porous medium. They used two phase model for nanofluid and considered the influences of activation energy and microorganisms.

The use of both nanofluid and porous media has attracted large amount of attention of the technologists due to advancement of heat transfer and it has directed to investigate extensively on this particular area. Motivated by the huge applications area of nanofluid flow and heat transfer past a stretching cylinder in porous medium, an attempt has been taken here to explore such problem with the help of single-phase model of nanofluid considering water as base fluid and Al_2O_3 as nanoparticles. This study remarkably inspects the flow and thermal behaviour of boundary layer axisymmetric Al_2O_3-water nanofluid flow over a stretching cylinder embedded in Darcy porous medium taking the combined effects of velocity slip and externally applied uniform magnetic field. According to the author's knowledge, no one has yet handled such problem. This focuses on the originality of the present research work. Using similarity transformations, momentum equation is converted to third order and heat equation is transformed to second order differential equations involving numerous dimensionless parameters of the problem. Numerical calculations are carried out with Runge-Kutta method via shooting technique and the results are presented through graphs and table. Detail analysis reveals that flow field and heat transfer are significantly influenced by the velocity slip parameter.

2. Formulation of the problem

Consider the steady axisymmetric boundary layer flow and heat transfer of nanofluid with Al_2O_3 as nanoparticles and water as base fluid past a horizontal stretching cylinder in porous medium in presence of uniform magnetic field applied in the perpendicular direction of the flow (see, Fig.1). During the heat transfer process, surface temperature of the cylinder i.e. temperature of the wall of the cylinder may remain uniform or it may vary with the distance. So, in this study, two types of surface temperature: Uniform Wall Temperature (UWT) and Variable Wall Temperature (VWT) are considered.

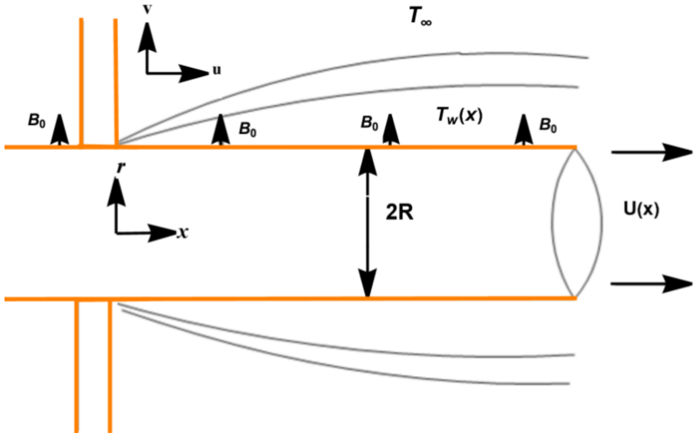

Fig1: Sketch of the physical flow problem

Generally, Darcy term is used in modelling flow through porous medium. According to Darcy (1856), the pressure gradient has a direct relationship with the volumetric flux of fluid across porous medium. Darcy's law suits well only when the velocity is low and the porosity of the medium is low [12]. Therefore, under boundary layer approximations, the governing equations and the associated boundary conditions can be written as follows[32, 33]:

2.1.1. Equations for fluid flow

$$\frac{\partial(ru)}{\partial x}+\frac{\partial(r\upsilon)}{\partial r}=0, \tag{1}$$

$$u\frac{\partial u}{\partial x}+\upsilon\frac{\partial u}{\partial r}=\frac{\nu_{nf}}{r}\frac{\partial}{\partial r}\left(r\frac{\partial u}{\partial r}\right)-\frac{\sigma_{nf}B_0^2}{\rho_{nf}}u-\frac{\nu_{nf}}{k_1}u. \tag{2}$$

2.1.2. Associated boundary conditions for fluid flow

$$u=U(x)+\mathrm{B}_1\nu_{nf}\frac{\partial u}{\partial r},\ \ \upsilon=0 \text{ at } r=R, \tag{3a}$$

$$u\to 0 \text{ as } r\to\infty. \tag{3b}$$

2.2.1. Equations for heat transfer

$$u\frac{\partial T}{\partial x}+\upsilon\frac{\partial T}{\partial r}=\frac{\kappa_{nf}}{(\rho c_p)_{nf}}\frac{1}{r}\frac{\partial}{\partial r}\left(r\frac{\partial T}{\partial r}\right), \tag{4}$$

2.2.2. Associated boundary conditions for heat transfer

Case-I: Uniform Wall Temperature (UWT):

The boundary conditions can be stated as

$$T=T_w \text{ at } r=R, \tag{5a}$$

$$T\to T_\infty \text{ as } r\to\infty. \tag{5b}$$

Case-II: Variable Wall Temperature (VWT):

For this case the appropriate boundary conditions are

$$T = T_w(x) = T_\infty + T_0\left(\frac{x}{L}\right)^{N} \text{ at } r = R, \tag{6a}$$

$$T \to T_\infty \text{ as } r \to \infty. \tag{6b}$$

Here, u and υ characterize the components of velocity respectively along the x and r -axes, $\nu_{nf} = \frac{\mu_{nf}}{\rho_{nf}}$ indicates the kinematic viscosity of nanofluid whereas dynamic viscosity of the same is μ_{nf} and ρ_{nf} signifies the density of the nanofluid, k_{nf} represents the effective thermal conductivity and $\left(\rho c_p\right)_{nf}$ stands for the effective heat capacitance, electrical conductivity of the nanofluid is σ_{nf} , k_1 denotes the permeability of the porous medium. T symbolizes the temperature and T_∞ denotes the free stream temperature. B_0 represents the uniform strength of the magnetic field. Here $U(x) = \frac{U_0 x}{L}$ is the stretching velocity while U_0 is the reference velocity, B_1 is the velocity slip, T_0 is the reference temperature and N represents the temperature exponent. Also, L denotes the characteristic length.

The effective fluid properties are given by [34, 35]:

$$\mu_{nf} = \frac{\mu_f}{(1-\phi)^{2.5}},\ \rho_{nf} = (1-\phi)\rho_f + \phi\rho_s,$$

$$\frac{k_{nf}}{k_f} = \frac{(k_s+2k_f)-2\phi(k_f-k_s)}{k_s+2k_f+\phi(k_f-k_s)},\ \left(\rho c_p\right)_{nf} = (1-\phi)\left(\rho c_p\right)_f + \phi\left(\rho c_p\right)_s \text{ and}$$

$$\sigma_{nf} = \sigma_f\left[1+\frac{3(\sigma-1)\phi}{(\sigma+2)-(\sigma-1)\phi}\right] \text{ where } \sigma = \frac{\sigma_s}{\sigma_f}. \tag{7}$$

Here, ϕ is the volume fraction of the nanoparticles. The subscripts *f*, *s*, and *nf* are used to mention the base fluid, solid nanoparticles and nanofluid respectively.

The thermophysical properties of water and Al_2O_3 are given in Table 1 [36].

Table 1: Thermophysical data for water and Al_2O_3 -nanoparticles

Physical Properties	Water	Al_2O_3
$\rho\ (kg/m^3)$	997.1	3970
$c_p\ (J/kgK)$	4179	765
$\kappa\ (W/mK)$	0.623	40
$\sigma\ (kg^{-1}m^{-3}s^3A^2)$	0.05	3.69×10^7

2.3. Similarity Transformations

Let us consider the subsequent similarity transformations [37],

$$u = \frac{1}{r}\frac{\partial\psi}{\partial r} \text{ and } \upsilon = -\frac{1}{r}\frac{\partial\psi}{\partial x}, \tag{8}$$

$$\eta = \frac{r^2-R^2}{2R}\sqrt{\frac{U}{\nu_f x}},\ \psi = \sqrt{U\nu_f x}\,Rf(\eta),\ \theta(\eta) = \frac{T-T_\infty}{T_w-T_\infty}. \tag{9}$$

With the use of (7)-(9), the governing equations reduce to

$$\frac{\mu_{nf}/\mu_f}{\rho_{nf}/\rho_f}(1+2\alpha\eta)f''' + \frac{\mu_{nf}/\mu_f}{\rho_{nf}/\rho_f}\left(2\alpha f'' - \mathrm{K}f'\right) + ff'' - f'^2 - \mathrm{M}\frac{\sigma_{nf}/\sigma_f}{\rho_{nf}/\rho_f}f' = 0, \tag{10}$$

$$\frac{1}{\Pr}\frac{\kappa_{nf}/\kappa_f}{\left(\rho c_p\right)_{nf}/\left(\rho c_p\right)_f}\left\{2\alpha\theta'+\left(1+2\alpha\eta\right)\theta''\right\}+f\theta'=0,\quad \textbf{[for I: UWT]} \tag{11}$$

$$\frac{1}{\Pr}\frac{\kappa_{nf}/\kappa_f}{\left(\rho c_p\right)_{nf}/\left(\rho c_p\right)_f}\left\{2\alpha\theta'+\left(1+2\alpha\eta\right)\theta''\right\}+f\theta'-\mathrm{N}f'\theta=0,\quad \textbf{[for II: VWT]} \tag{12}$$

where $\alpha=\sqrt{\dfrac{\nu_f L}{U_0R^2}}$ is the curvature parameter, $\mathrm{K}=\dfrac{\nu_f L}{U_0 k_1}$ is the parameter of the porous medium and magnetic parameter is $\mathrm{M}=\dfrac{B_0^2 L\sigma_f}{U_0\rho_f}$. The Prandtl number is denoted by $\Pr=\dfrac{\left(\mu c_p\right)_f}{\kappa_f}$.

The boundary conditions become,

$$f'(\eta)=1+\frac{\nu_{nf}}{\nu_f}\mathrm{B}f''(\eta),\; f(\eta)=0,\; \theta(\eta)=1 \quad \text{at } \eta=0, \tag{13}$$

$$\text{and}\quad f'\to 0,\;\theta\to 0 \quad \text{as}\quad \eta\to\infty, \tag{14}$$

where $\mathrm{B}=\mathrm{B}_1\sqrt{\dfrac{U_0\nu_f}{L}}$ denotes the slip parameter.

3. Numerical computations

The above equations (10), (11) or (12) along with the boundary conditions (13)-(14) are solved by altering them to an initial value problem (IVP). For this we put

$$\begin{cases} f' = z, \\ z' = p, \\ p' = \dfrac{\rho_{nf}/\rho_f}{\mu_{nf}/\mu_f}\dfrac{1}{\left(1+2\alpha\eta\right)}\left(z^2-fp-\dfrac{\mu_{nf}/\mu_f}{\rho_{nf}/\rho_f}(2\alpha p-\mathrm{K}z)+\mathrm{M}\dfrac{\sigma_{nf}/\sigma_f}{\rho_{nf}/\rho_f}z\right), \end{cases} \tag{15}$$

$$\begin{cases} \theta' = q, \\ q' = \dfrac{\Pr\left(\rho c_p\right)_{nf}/\left(\rho c_p\right)_f}{\left(1+2\alpha\eta\right)\dfrac{\kappa_{nf}}{\kappa_f}}\left\{\left(-\dfrac{1}{\Pr}\dfrac{\kappa_{nf}/\kappa_f}{\left(\rho c_p\right)_{nf}/\left(\rho c_p\right)_f}2\alpha q\right)-fq\right\}, \end{cases} \quad \text{(for UWT)} \tag{16a}$$

$$\begin{cases} \theta' = q, \\ q' = \dfrac{\Pr\left(\rho c_p\right)_{nf}/\left(\rho c_p\right)_f}{\left(1+2\alpha\eta\right)\dfrac{\kappa_{nf}}{\kappa_f}}\left(-\dfrac{1}{\Pr}\dfrac{\kappa_{nf}/\kappa_f}{\left(\rho c_p\right)_{nf}/\left(\rho c_p\right)_f}2\alpha q-\left(fq-\mathrm{N}z\theta\right)\right), \end{cases} \quad \text{(for VWT)} \tag{16b}$$

The boundary conditions are

$$f'(0)=1+\frac{\nu_{nf}}{\nu_f}\mathrm{B}f''(0),\; f(0)=0,\; \theta(0)=1 \tag{17}$$

To integrate the equations (15), (16a) or (16b) as an IVP one needs $p(0)$ i.e. $f''(0)$ and $q(0)$ i.e. $\theta'(0)$ but there are no such values. The guess these values $f''(0)$ and $\theta'(0)$ are selected for performing the integration. Comparing the computed data of f' and θ at $\eta=\eta_\infty=8$ (say) with the specified boundary conditions and also adjusting the guess values of $f''(0)$ and $\theta'(0)$ appropriate numerical computations are conducted. Sequences of values for $f''(0)$, $\theta'(0)$ are selected in this case and Runge-Kutta method of fourth order with a step size of h=0.01

is used. This numerical procedure is repeated until the converged results are received within a limit of 10^{-6}. Detailed phases for the numerical calculations have been revealed in Fig.2.

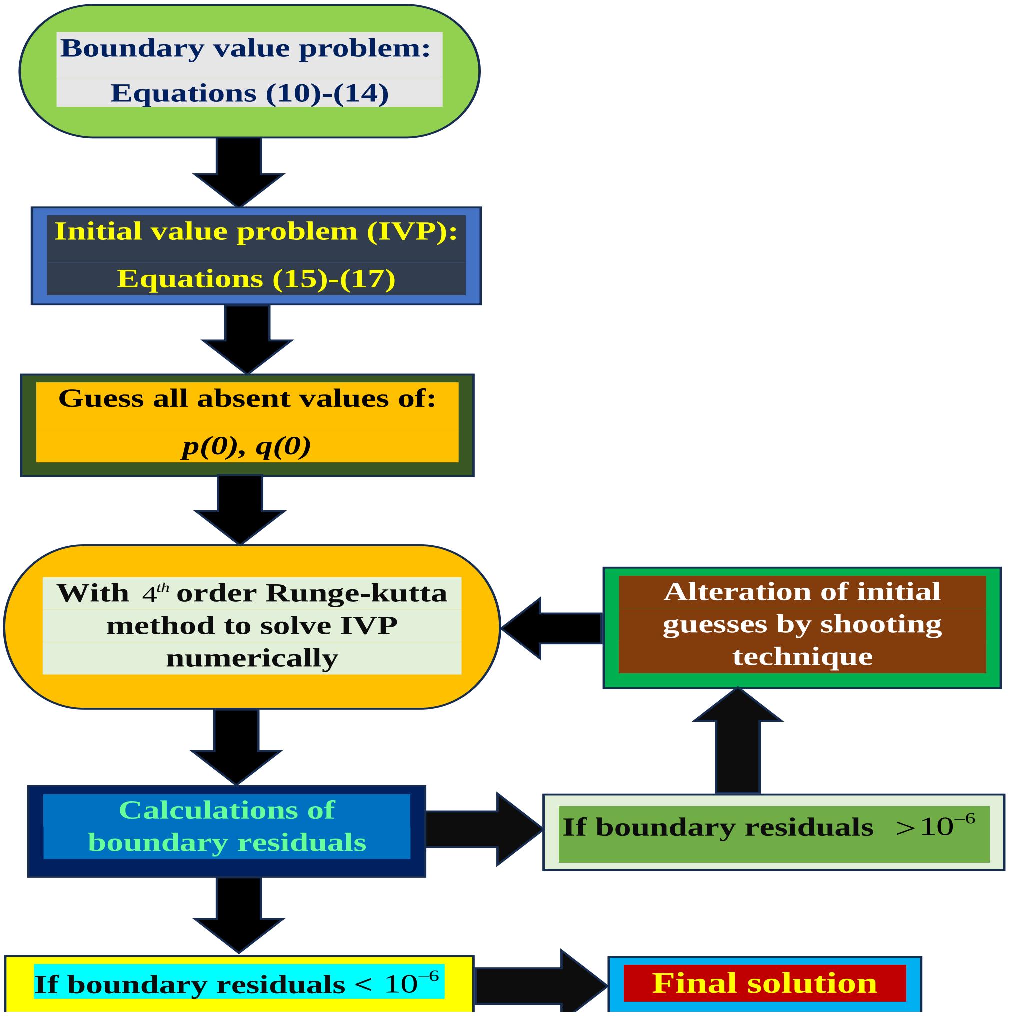

Fig2: Phases for numerical calculations

3.1. Validation of results

To examine the accuracy of the method used in this study, the data for $[-\theta'(0)]$ are matched up with the existing data of Grubka and Bobba [38], Ali [39], Ishak and Nazar [40] and Mukhopadhyay et al. [37] for the various values of temperature exponent N as stated in Table 2. Our outcomes are in perfect agreement with their results and this gives us immense confidence to carry on the numerical computations for other parametric values. Moreover, none of them considered nanofluid flow in porous medium. Therefore, the present findings are different from their publications as our results are for nanofluid flow past a stretching cylinder in porous medium. So, more important and attractive features regarding flow and heat transfer behavior have been reported in our study.

4. Results and discussions

To provide a complete analysis of nanofluid flow and heat transport over a horizontal stretching surface, numerical data are presented through Figs 3(a)-8(c) and Tables 2-3. The main intention is to accomplish better idea about the fluid flow problem. For this purpose, firstly, the influences of α (curvature parameter) on fluid velocity in cases of slip and no-slip at the boundary are presented through Fig.3(a). Horizontal velocity exhibits that the rate of transfer of momentum reduces with the rising distance η commencing from the sheet. In both cases, the velocity reaches to zero at some larger distance from the sheet (nearly at $\eta = 10$). In the absence of slip, flow velocity rises with the rise in curvature parameter α [Fig.3(a)] which is consistent with the findings of Mukhopadhyay [27]. However, in presence of slip, the velocity declines at first (near the surface) but after a certain distance from the wall (just after the crossing over point), it augments with swelling values of α [Fig.3(a)]. Initially, the velocity declines owing to slip at the wall. Higher velocity is observed for no-slip at the boundary compared to slip [Fig.3(a)]. It is noted that 31.64% increase in fluid velocity occurs at η=2 when the curvature parameter increases its value from 0.1 to 0.9 in presence of slip (when B=0.5). Such result has various applications in engineering sectors. For example, in microfluidic devices, slip at the boundary assists to decrease drag and thus helps to advance the movement of fluid through channels of micro diameter. Temperature is noted to increase with the growing values of curvature parameter α [Fig.3(b)]. This impact is higher in case of slip at the boundary [Fig.3(b)] compared to the no-slip case [Fig.3(b)]. Basically, with the change in α, lateral surface of the cylinder changes which has significant impact on velocity as well as temperature. 31.25% rise in fluid temperature happens at η=0.7 when α rises its value from 0.1 to 0.9 for the case of B=0.5.

Table 2: Values of $[-\theta'(0)]$ for some values of temperature exponent N

N	Grubka and Bobba [38]	Ali [39]	Ishak and Nazar [40]	Mukhopadhyay et al. [37] $(\lambda=B=M=0, Pr=1)$	Present results $\begin{pmatrix} M=K=B=0, \\ \alpha=\phi=0, Pr=1 \end{pmatrix}$
0	0.5820	0.5801	0.5820	0.5821	0.581977
1	1.0000	0.9961	1.0000	1.0000	1.00000
2	1.3333	1.3269	1.3333	1.3332	1.33333

Influences of nanoparticle volume fraction ϕ on $f'(\eta)$ and $\theta(\eta)$ are displayed through Figs.4(a)-(b) respectively. Velocity decreases due to rise in ϕ for both cases of slip and no-slip [Fig.4(a)]. Basically, with the rise in ϕ, frictional force increases and so fluid velocity diminishes. Compared to slip, higher velocity is observed for no-slip boundary condition [Fig.4(a)]. Fluid velocity decreases 1.13% at η=2 when nanoparticle volume fraction increases from 0.0 to 0.06 in presence of slip (with B=0.8). Fluid temperature is found to increase for mounting values of ϕ. Higher temperature is observed in case of slip compared to no-slip case [Fig.4(b)]. When the nanoparticle volume fraction increases from 0.0 to 0.06, fluid temperature increases by 36.19% at η=1.2 when there is slip (B=0.8).

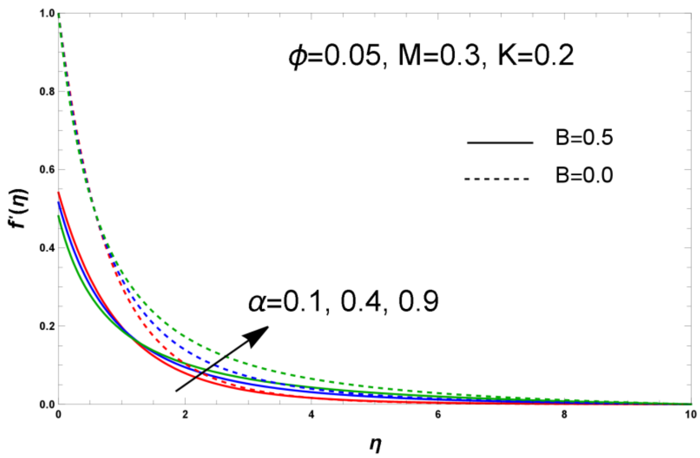

Fig.3(a): Effects of α on $f'(\eta)$

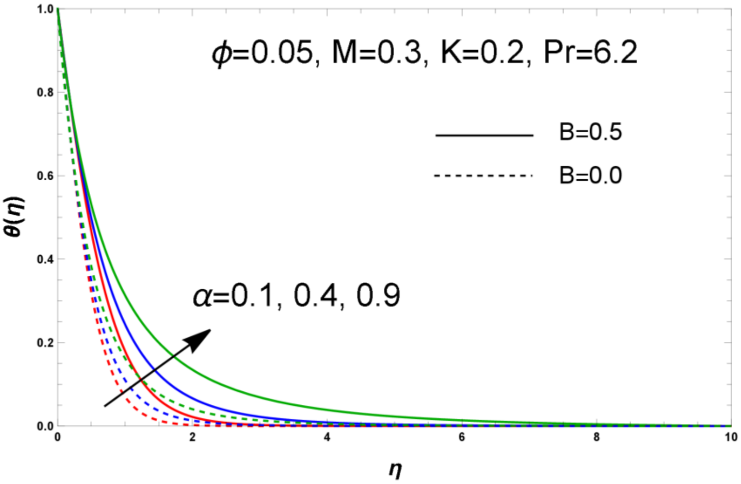

Fig.3(b): Effects of α on $\theta(\eta)$

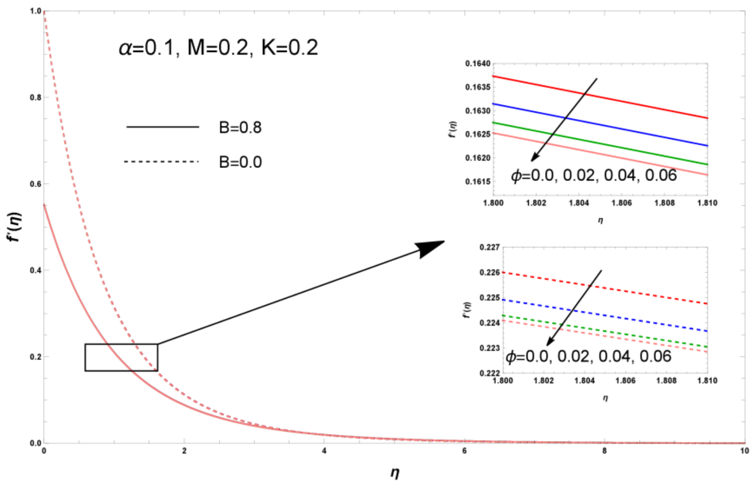

Fig.4(a): Effects of ϕ on $f'(\eta)$

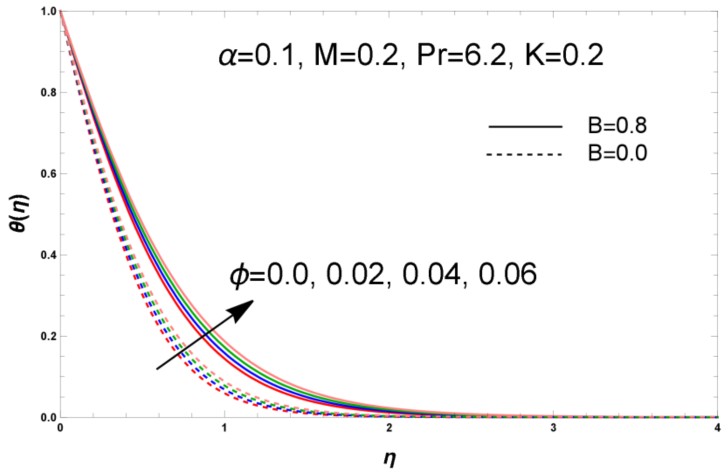

Fig.4(b): Effects of ϕ on $\theta(\eta)$

The impacts of slip parameter B on velocity and temperature are shown in Figs.5(a)-(b) for both presence of magnetic field (i.e. M=0.3) and absence of magnetic field (i.e. for M=0). Due to slip parameter B, the velocity of the fluid diminishes initially but far away from the wall, it is found to augment for both presence of magnetic field (i.e. M=0.3) and also in the absence of magnetic field (i.e. for M=0) [Fig.5(a)]. There is a variance between flow velocity near a stretching wall and the stretching velocity of the wall when slip occurs. As the value of B rises, the slip velocity increases, leading to a decline in fluid velocity. This reduction in flow velocity happens as under slip condition the dragging motion of the stretching wall can only be partially transmitted to the fluid [37]. Compared to no-slip case, 23.3% decrease in flow velocity is found at η=2 with slip (B=0.8) in presence of magnetic field. Temperature rises with growing values of slip parameter B for both cases of M=0.3 and M=0. Also, superior temperature distribution is noted for presence of magnetic field [Fig.5(b)]. Compared to no-slip case, 11.76% rise in fluid temperature is observed at η=0.2 with slip (B=0.8) for M=0.3.

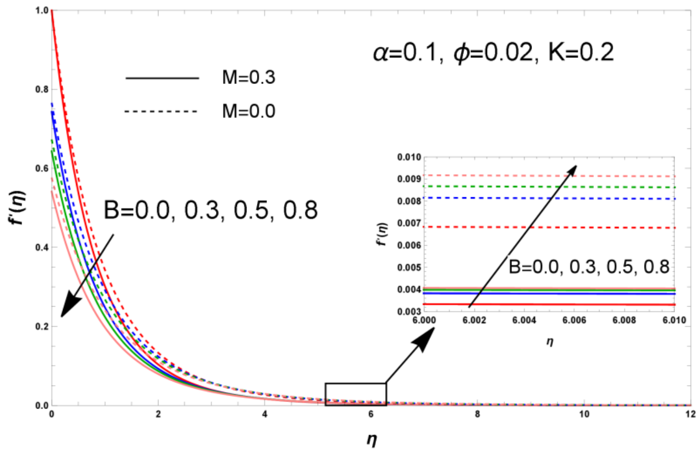

Fig.5(a): Effects of B on $f'(\eta)$

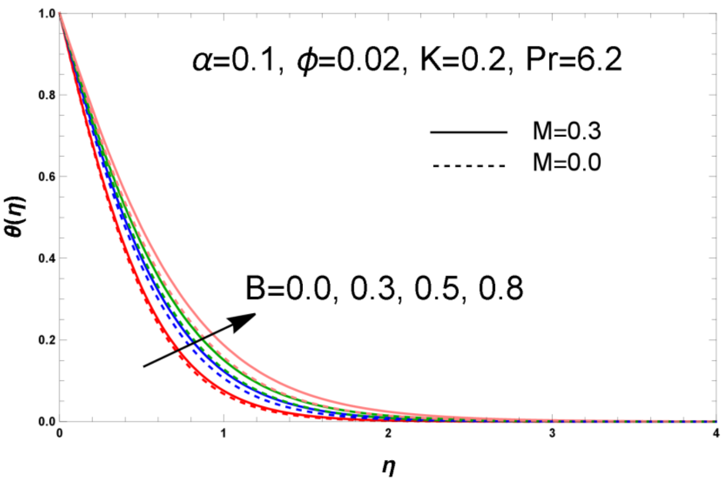

Fig.5(b): Effects of B on $\theta(\eta)$

Consequences of magnetic parameter M on fluid velocity and hotness field are stated respectively by Fig.6(a) and Fig.6(b). From Fig.6(a) we see that the momentum boundary layer thickness declines for the increasing M. Actually, with the mounting M, Lorentz rises and this force opposes the fluid flow. Therefore, velocity reduces with the rise in magnetic parameter M [Fig.6(a)]. Compared to slip, higher velocity is detected for no-slip condition [Fig.6(a)]. 42% reduction in flow velocity is noted at η=2 when the magnetic parameter M increases its value from 0.2 to 0.8 in the presence of slip (when B=0.5). For both slip and no-slip cases, fluid temperature enlarges with the increasing values of M leading to rise in thermal boundary layer thickness [Fig.6(b)]. Here, compared to no-slip, for slip superior temperature is perceived [Fig.6(b)]. 15.35% increase in temperature is found at η=0.7 when the magnetic parameter rises its value from 0.2 to 0.8 for B=0.5.

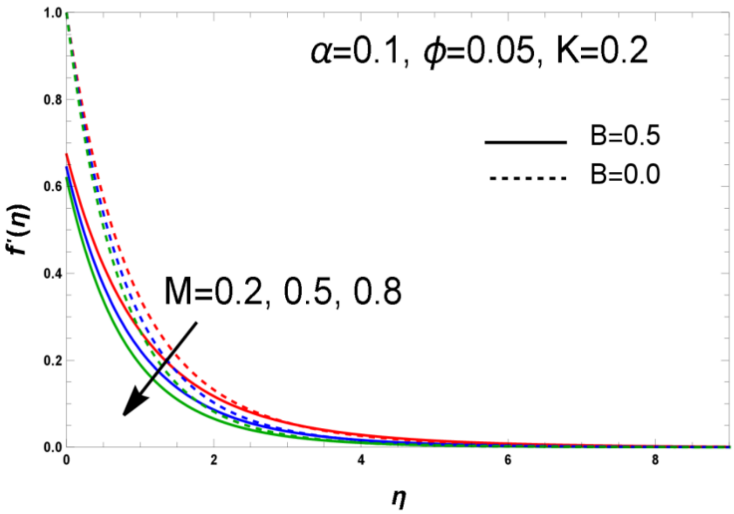

Fig.6(a): Effects of M on $f'(\eta)$

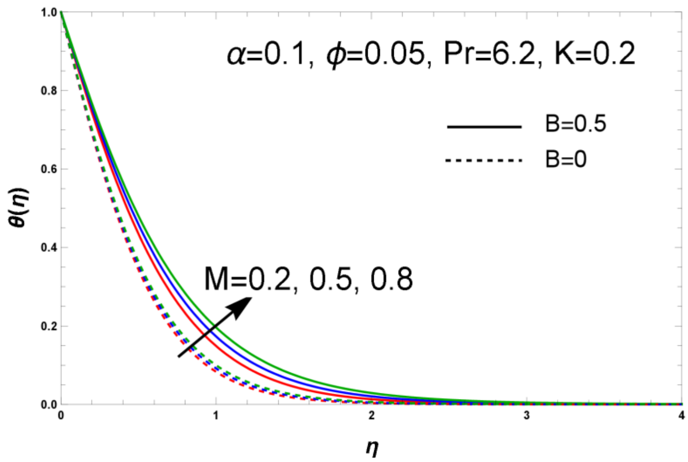

Fig.6(b): Effects of M on $\theta(\eta)$

Fluid velocity diminishes with the rise in permeability parameter K of the porous medium [Fig.7(a)]. Higher velocity is observed for no-slip case [Fig.7(a)]. 32.95% drop in fluid velocity is detected at η=2 when the permeability parameter K enhances its value from 0.1 to 0.5 in the presence of slip. Temperature is found to rise with the rising permeability parameter [Fig.7(b)]. Compared to no-slip case, higher temperature is noted for slip case [Fig.7(b)]. Basically, the permeability of the medium represents the ability of the material of the porous medium to allow the fluid particles to pass through it. Moreover, permeability parameter K is inversely proportional to the permeability of the porous medium k_1 which can be found from the expression $\mathrm{K} = \frac{\nu_f L}{U_0 k_1}$. So, rising values of permeability parameter K restrict the fluid flow as the permeability of the medium (k_1) diminishes in this case. As a result, with the enhancing values of the permeability parameter, the restriction to the movement of nanofluid rises which slows down the fluid flow. So, the temperature rises in this case. 50% increment in fluid temperature is noted at η=2 when the permeability parameter K rises its value from 0.1 to 0.5 in the absence of slip.

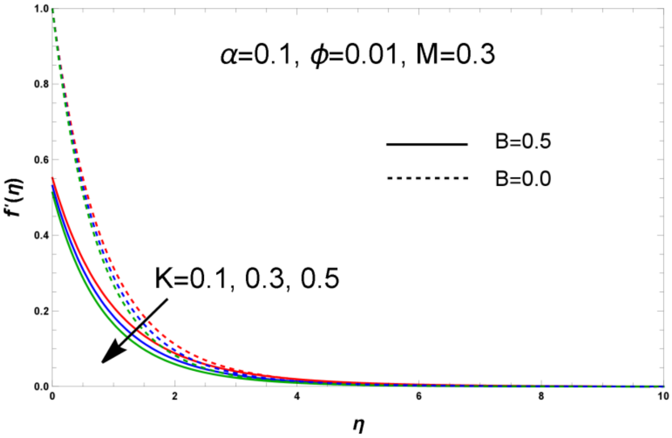

Fig.7(a): Effects of K on $f'(\eta)$

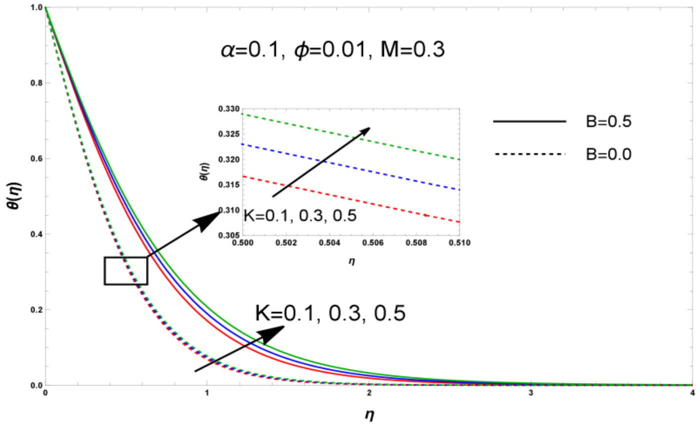

Fig.7(b): Effects of K on $\theta(\eta)$

Fluid temperature is noted to decline for rising values of temperature exponent parameter N for both slip and no-slip boundary conditions, also compared to no-slip, advanced temperature is remarked for slip case [Fig.8]. Also, temperature overshoot is observed near the surface for $N = -1.5$ [Fig.8]. 40.9% reduce in the temperature of the fluid occurs at η=1.5 when the temperature exponent parameter N rises its value from -1.5 to -1 for B=0.5.

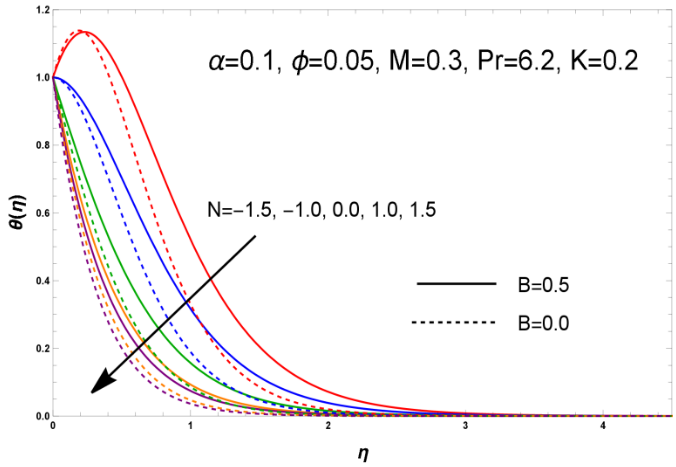

Fig.8: Effects of N on $\theta(\eta)$

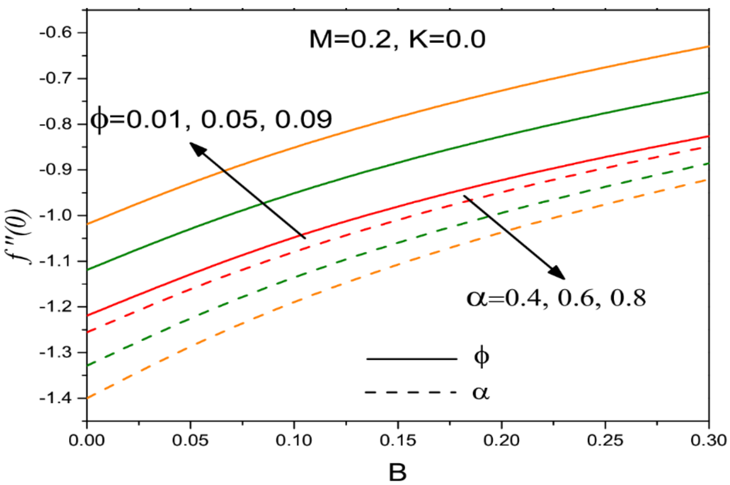

Fig.9(a): Variation of $f''(0)$ with B for several values of ϕ and α

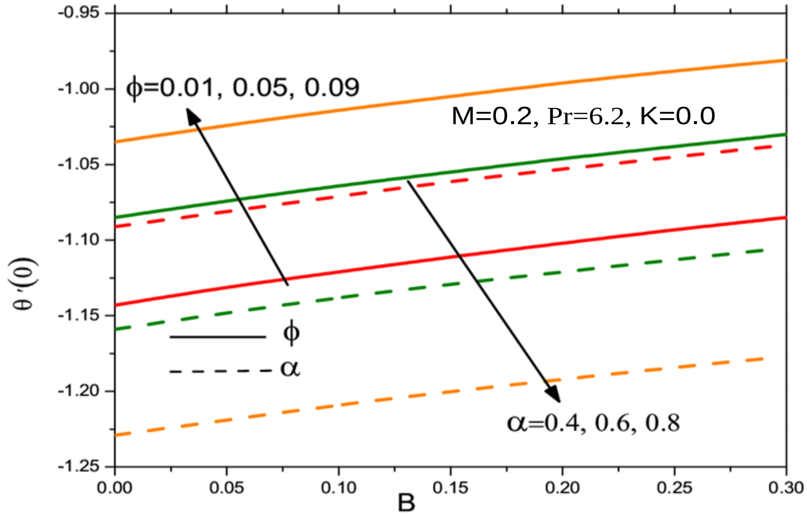

Fig.9(b): Variation of $\theta'(0)$ with B for several values of ϕ and α

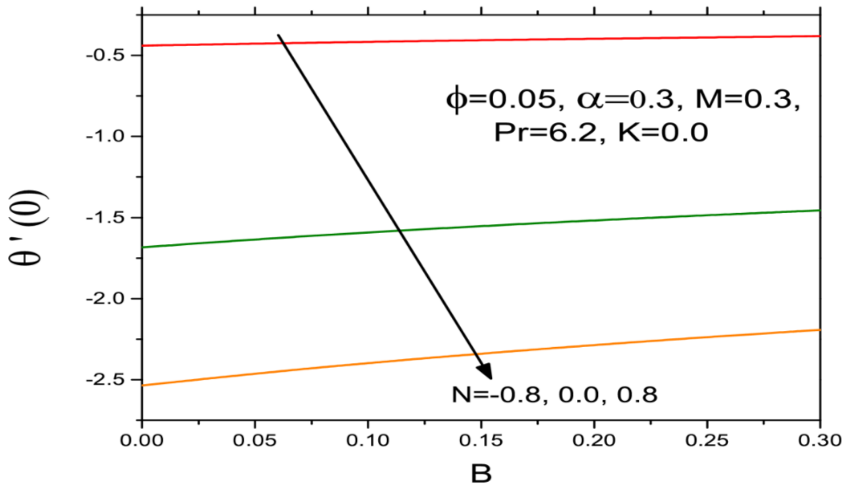

Fig.9(c): Variation of $\theta'(0)$ with B for several values of N

Velocity gradient at the surface $f''(0)$ rises with the swelling of ϕ and $f''(0)$ declines with the growing values of α [Fig.9(a)]. Also, $f''(0)$ rises with the boosting values of B [Fig.9(a)]. In the absence of slip (i.e., B=0), 16.67% increase in velocity gradient is observed when ϕ rises its value from 0.01 to 0.09 and 8.3% reduction in velocity gradient is noted when α rises its value from 0.4 to 0.8. For slip at the boundary, a relative motion between the nanofluid and the surface occurs which creates a flow resistance and it increases as slip increases at the boundary. The figure displays that shear stress at the wall is negative. Physically, negative sign of $f''(0)$ indicates that the surface pulls the fluid, and a positive sign specifies that the surface releases fluid. Temperature gradient at the surface $\theta'(0)$ is initiated to diminish with the swelling values of α but $\theta'(0)$ rises with the growing values of ϕ and B [Fig.9(b)]. This result can be used for cooling purposes, for example, cooling of heat exchangers, cooling of turbine blade etc. It is obvious that the heat transfer rate at the surface reduces with the rise in ϕ since Nusselt number [given by $Nu = \frac{-\theta'(0)}{\sqrt{\mathrm{Re}}}$] reduces when $\theta'(0)$ rises with the rise in ϕ. 23.3% enhance and 12.64% decrease in temperature gradient is noticed when the nanoparticle volume fraction enhances from 0.01 to 0.09 and α rises its value from 0.4 to 0.8, specifically in the absence of slip. From Fig.9(c), it is found that $\theta'(0)$ reduces for escalating values of temperature exponent N, while it slightly increases for the mounting values of B. These findings fully agree with the specified data provided in Table 3. It is to be noted that 50.6% decrease in temperature gradient occurs at B=0 when N rises its value from 0.0 to 0.8.

With the rise in K, $f''(0)$ and $\theta'(0)$ both are found to diminish [Table 3]. With the rise in permeability parameter K of the porous medium, reduction in the Darcy body force (in magnitude) occurs as the Darcy body force is inversely proportional to the permeability parameter. Basically, Darcy body force acts as a resistive force which causes to decelerate the fluid particles. This resistance diminishes as permeability parameter K of the medium increases. So, the fluid flow experiences progressively less drag. Heat transfer rate at the surface rises as $\theta'(0)$ reduces with the rise in K [Table 3].

5. Conclusions

The objective of this study is to explore the MHD flow of Al_2O_3-water nanofluid past a horizontal stretching cylinder in porous medium under the influence of velocity slip at the boundary. Two types of surface temperature: Uniform Wall Temperature (UWT) and Variable Wall Temperature (VWT) have been considered in this study to explore the heat transfer characteristics clearly. Boundary layer axisymmetric flow and thermal behaviour of Al_2O_3-water nanofluid over a stretching cylinder embedded in Darcy porous medium taking the combined effects of velocity slip and externally applied uniform magnetic field has not yet been addressed by any researcher and thus it indicates the novelty of the present research. Similarity transformations have been used to obtain the self-similar solutions and numerical solutions of the problem under consideration are obtained taking the help of Runge-Kutta method with Shooting technique. The effects of the different parameters on flow and thermal behaviours have been carefully inspected and reported in detail. Owing to slip parameter, fluid velocity reduces near the surface but rises away from the wall. Temperature is enhanced with growing values of slip parameter. The curvature parameter of the stretching cylinder plays a vital role by influencing the flow and temperature field significantly. The velocity gradient at the surface and the temperature gradient at the surface both are found to reduce as the curvature parameter rises. Most importantly, it is found that reduction in the temperature of the fluid reduces 40.9% at η=1.5 when temperature exponent parameter N rises -1.5 to -1 for B=0.5. This result has important aspect as it can be used for cooling purpose by considering Variable Wall Temperature for heat transfer problem.

This research contributes to the understanding of MHD nanofluid flow past a stretching cylinder in porous medium in presence of slip and highlights the capacity for optimizing heat transfer in manufacturing systems.

Acknowledgements

One of the authors (S. D.) classifies the financial assistance permitted from UGC through UGC-SRF (NTA Ref. No. 211610113714). Authors are thankful to the reviewers for constructive suggestions.

Table 3: Values of $f''(0)$, $\theta'(0)$ for M=0.4

ϕ	α	B	N	K	Pr	$f''(0)$	$\theta'(0)$
0	0	0	0	0.2	3.2	-1.26491	-1.15279
		0.2				-0.959055	-1.02559
		0.4				-0.780515	-0.937443
			0.2				-1.08118
			0.4				-1.21565
0.01	0.1	0	0			-1.31013	-1.15772
		0.2				-0.988132	-1.02869
		0.4				-0.801644	-0.939661
			0.2				-1.08221
			0.4				-1.21531
0.02		0.2				-0.989968	-1.30425
		0.4				-0.80331	-1.19267
			0.2				-1.06176
			0.4				-1.19267
				0.3		-0.82191	-1.17456
				0.4		-0.839561	-1.15713
				0.5		-0.856357	-1.14034
					4.2		-1.34761
					5.2		-1.53119
					6.2		-1.69763
			-0.2				-1.10838
			-0.4				-0.876463

References

[1] S. Hosseinzadeh, K. Hosseinzadeh, A. Hasibi, D. Ganji, Hydrothermal analysis on non-Newtonian nanofluid flow of blood through porous vessels, *Proceedings of the Institution of Mechanical Engineers, Part E: Journal of Process Mechanical Engineering,* Vol. 236, No. 4, pp. 1604-1615, 2022.

[2] N. Alipour, B. Jafari, K. Hosseinzadeh, Optimization of wavy trapezoidal porous cavity containing mixture hybrid nanofluid (water/ethylene glycol Go–Al2O3) by response surface method, *Scientific Reports,* Vol. 13, No. 1, pp. 1635, 2023.

[3] M. F. Najafabadi, H. TalebiRostami, K. Hosseinzadeh, D. Ganji, Investigation of nanofluid flow in a vertical channel considering polynomial boundary conditions by Akbari-Ganji's method, *Theoretical and Applied Mechanics Letters,* Vol. 12, No. 4, pp. 100356, 2022.

[4] K. Hosseinzadeh, M. Mardani, S. Salehi, M. Paikar, D. Ganji, Investigation of micropolar hybrid nanofluid (iron oxide–molybdenum disulfide) flow across a sinusoidal cylinder in presence of magnetic field, *International Journal of Applied and Computational Mathematics,* Vol. 7, pp. 1-17, 2021.

[5] M. R. Zangooee, K. Hosseinzadeh, D. D. Ganj, Investigation of three-dimensional hybrid nanofluid flow affected by nonuniform MHD over exponential stretching/shrinking plate, *Nonlinear Engineering*, Vol. 11, No. 1, pp. 143-155, 2022.

[6] M. Fallah Najafabadi, H. Talebi Rostami, K. Hosseinzadeh, D. D. Ganji, Hydrothermal study of nanofluid flow in channel by RBF method with exponential boundary conditions, *Proceedings of the Institution of Mechanical engineers, Part E: Journal of process Mechanical engineering,* Vol. 237, No. 6, pp. 2268-2277, 2023.

[7] S. U. Choi, J. A. Eastman, *Enhancing thermal conductivity of fluids with nanoparticles*, Argonne National Lab.(ANL), Argonne, IL (United States), pp. 1995.

[8] Y. Xuan, Q. Li, Heat transfer enhancement of nanofluids, *International Journal of heat and fluid flow,* Vol. 21, No. 1, pp. 58-64, 2000.

[9] S. Z. Heris, S. G. Etemad, M. N. Esfahany, Convective heat transfer of a Cu/water nanofluid flowing through a circular tube, *Experimental heat transfer,* Vol. 22, No. 4, pp. 217-227, 2009.

[10] S. Mukhopadhyay, Heat transfer analysis for unsteady MHD flow past a non-isothermal stretching surface, *Nuclear engineering and design,* Vol. 241, No. 12, pp. 4835-4839, 2011.

[11] S. Nadeem, S. Hussain, Flow and heat transfer analysis of Williamson nanofluid, *Applied Nanoscience,* Vol. 4, pp. 1005-1012, 2014.

[12] S. Hameed, S. Saha, Analysis of mixed convecto-magnetic Buongiorno nanofluid flow in a non-Darcy porous medium, *Journal of Taibah University for Science,* Vol. 17, No. 1, pp. 2233755, 2023.

[13] A. Kasaeian, R. Daneshazarian, O. Mahian, L. Kolsi, A. J. Chamkha, S. Wongwises, I. Pop, Nanofluid flow and heat transfer in porous media: a review of the latest developments, *International Journal of Heat and Mass Transfer,* Vol. 107, pp. 778-791, 2017.

[14] H. I. Andersson, Slip flow past a stretching surface, *Acta Mechanica,* Vol. 158, No. 1, pp. 121-125, 2002.

[15] Z. Abbas, Y. Wang, T. Hayat, M. Oberlack, Slip effects and heat transfer analysis in a viscous fluid over an oscillatory stretching surface, *International Journal for Numerical Methods in Fluids,* Vol. 59, No. 4, pp. 443-458, 2009.

[16] S. Mukhopadhyay, Effects of slip on unsteady mixed convective flow and heat transfer past a porous stretching surface, *Nuclear Engineering and Design,* Vol. 241, No. 8, pp. 2660-2665, 2011.

[17] J. Gbadeyan, E. Titiloye, A. Adeosun, Effect of variable thermal conductivity and viscosity on Casson nanofluid flow with convective heating and velocity slip, *Heliyon,* Vol. 6, No. 1, 2020.

[18] M. Sheikholeslami, D. D. Ganji, M. Y. Javed, R. Ellahi, Effect of thermal radiation on magnetohydrodynamics nanofluid flow and heat transfer by means of two phase model, *Journal of magnetism and Magnetic materials,* Vol. 374, pp. 36-43, 2015.

[19] S. Ghosh, S. Mukhopadhyay, MHD slip flow and heat transfer of Casson nanofluid over an exponentially stretching permeable sheet, *International Journal of Automotive and Mechanical Engineering,* Vol. 14, No. 4, pp. 4785-4804, 2017.

[20] S. Dey, S. Mukhopadhyay, MHD nanofluid flow over an absorbent plate in the company of chemical response and zero nanoparticle flux, *Forces in Mechanics,* Vol. 7, pp. 100102, 2022.

[21] K. A. Khan, M. F. Javed, M. A. Ullah, M. B. Riaz, Heat and Mass transport analysis for Williamson MHD nanofluid flow over a stretched sheet, *Results in Physics,* Vol. 53, pp. 106873, 2023.

[22] M. Naveed Khan, A. Alhowaity, Z. Wang, K. A. Gepreel, M. Hussien, Numerical analysis of the heat transfer application on a convective tangent hyperbolic nanofluid flow over a porous stretching cylinder with stratification effects, *Numerical Heat Transfer, Part A: Applications*, pp. 1-17, 2024.

[23] M. I. Sulaiman Basha, D. M. G. Anthony, Numerical investigation of non-linear radiative flow of hybrid nanofluid past a stretching cylinder with inclined magnetic field, *Numerical Heat Transfer, Part B: Fundamentals,* Vol. 85, No. 7, pp. 842-866, 2024.

[24] A. Paul, N. Sarma, B. Patgiri, Numerical assessment of MHD thermo-mass flow of Casson ternary hybrid nanofluid around an exponentially stretching cylinder, *BioNanoScience,* pp. 1-16, 2024.

[25] C. Y. Wang, Fluid flow due to a stretching cylinder, *Physics of Fluids,* Vol. 31, No. 3, pp. 466-468, 1988.

[26] A. Ishak, R. Nazar, I. Pop, Uniform suction/blowing effect on flow and heat transfer due to a stretching cylinder, *Applied Mathematical Modelling,* Vol. 32, No. 10, pp. 2059-2066, 2008.

[27] S. Mukhopadhyay, MHD boundary layer slip flow along a stretching cylinder, *Ain Shams Engineering Journal,* Vol. 4, No. 2, pp. 317-324, 2013.

[28] H. Ashorynejad, M. Sheikholeslami, I. Pop, D. Ganji, Nanofluid flow and heat transfer due to a stretching cylinder in the presence of magnetic field, *Heat and Mass Transfer*, Vol. 49, pp. 427-436, 2013.

[29] M. Tamoor, M. Waqas, M. I. Khan, A. Alsaedi, T. Hayat, Magnetohydrodynamic flow of Casson fluid over a stretching cylinder, *Results in physics*, Vol. 7, pp. 498-502, 2017.

[30] A. Mishra, M. Kumar, Velocity and thermal slip effects on MHD nanofluid flow past a stretching cylinder with viscous dissipation and Joule heating, *SN Applied Sciences*, Vol. 2, No. 8, pp. 1350, 2020.

[31] C. Sowmiya, B. R. Kumar, MHD Maxwell nanofluid flow over a stretching cylinder in porous media with microorganisms and activation energy, *Journal of Magnetism and Magnetic Materials*, Vol. 582, pp. 171032, 2023.

[32] S. Mukhopadhyay, A. Ishak, Mixed convection flow along a stretching cylinder in a thermally stratified medium, *Journal of Applied Mathematics*, Vol. 2012, No. 1, pp. 491695, 2012.

[33] N. Roşca, A. Roşca, I. Pop, J. Merkin, Nanofluid flow by a permeable stretching/shrinking cylinder, *Heat and Mass Transfer*, Vol. 56, pp. 547-557, 2020.

[34] S. Das, R. Jana, Natural convective magneto-nanofluid flow and radiative heat transfer past a moving vertical plate, *Alexandria Engineering Journal*, Vol. 54, No. 1, pp. 55-64, 2015.

[35] S. Konai, S. Mukhopadhyay, Insight into the Forced Convective Radiative Stefan flow of Nanofluid over an Unsteady Stretched Sheet, *International Journal of Computational Materials Science and Engineering*, 2024.

[36] R. Parveen, T. R. Mahapatra, Heat and mass source effect on MHD double-diffusive mixed convection and entropy generation in a curved enclosure filled with nanofluid, *Nonlinear Analysis: Modelling and Control*, Vol. 27, No. 2, pp. 308-330, 2022.

[37] S. Mukhopadhyay, P. R. De, K. Bhattacharyya, G. Layek, Slip effects on mixed convection flow along a stretching cylinder, *International Journal of Heat and Technology*, Vol. 30, No. 2, pp. 19-24, 2012.

[38] L. Grubka, K. Bobba, Heat transfer characteristics of a continuous stretching surface with variable temperature, *Journal of Heat Transfer*, Vol. 107, No. 1, pp. 248-250, 1985.

[39] M. E. Ali, Heat transfer characteristics of a continuous stretching surface, *Wärme-und Stoffübertragung*, Vol. 29, No. 4, pp. 227-234, 1994.

[40] A. Ishak, R. Nazar, Laminar boundary layer flow along a stretching cylinder, *European Journal of Scientific Research*, Vol. 36, No. 1, pp. 22-29, 2009.